IEEE Access
Multidisciplinary | Rapid Review | Open Access Journal

Received 5 May 2024, accepted 20 June 2024, date of publication 24 June 2024, date of current version 18 July 2024.

Digital Object Identifier 10.1109/ACCESS.2024.3418718

RESEARCH ARTICLE

A Ka-Band Beam-Steering Radar Transmitter Using Active Multiplier and Coupled Delay Line Phase Shifter

KYU-JIN CHOI[1], (Graduate Student Member, IEEE), REEM SONG[2], (Member, IEEE), CHAN-JONG LEE[3], JEONG-BAE YOON[1], (Student Member, IEEE), DONG-YEOL YANG[1], (Student Member, IEEE), SEUK-WON KANG[1], (Student Member, IEEE), SANGWOOK NAM[4], (Senior Member, IEEE), AND BYUNG-SUNG KIM[5], (Member, IEEE)

[1]Department of Electrical and Computer Engineering, Sungkyunkwan University, Suwon 16419, South Korea
[2]College of Information and Communication Engineering, Sungkyunkwan University, Suwon 16419, South Korea
[3]Research and Development Division, LG Electronics Inc., Seoul 06772, South Korea
[4]College of Electrical and Computer Engineering, Institute of New Media Communication, Seoul National University, Seoul 08826, South Korea
[5]Department of Semiconductor Systems Engineering, Sungkyunkwan University, Suwon 16419, South Korea

Corresponding author: Byung-Sung Kim (bskimice@skku.edu)

This work was supported by Samsung Electronics Company Ltd., under Grant IO201209-07913-01.

ABSTRACT This paper presents a Ka-band beam steering transmitter exploiting a coupled varactor loaded transmission line (VLTL) phase shifter and a CMOS transmitter chip with an integrated frequency multiplier. The short-coupled line couplers placed along a single VLTL provides multi-phase outputs while minimizing the impedance mismatch and unequal power distribution along the VLTLs. The inherent phase-accumulating nature along the VLTL reduces the burden of wide phase control range required for using separate phase shifters for each channel. Additionally, the frequency multiplier with a multiplication ratio of 8 reduces the required amount of phase change at the reference frequency and therefore the tuning range of the varactor, which also minimize a change of line characteristic impedance to ensure the impedance matching of the VLTL. Hence, a 32 GHz phased array transmitter is implemented using a single VLTL phase shifter operating at a low reference frequency of about 4 GHz. The fabricated 1×4 phased array transmitter achieves a continuous beam steering range of $\pm 20°$ in the E-plane using a single control voltage. The sidelobe level is below -10 dB at all scan angles and the peak effective isotropic radiated power (EIRP) is 38.1 dBm at 31.6 GHz and the 3-dB bandwidth of 2.4 GHz is achieved.

INDEX TERMS Phased-array, VLTL, beam-steering, coupler, phase shifter, transmitter, beamforming, loaded transmission line, effective isotropic radiated power (EIRP).

I. INTRODUCTION

Beamforming transmitters are widely used in wireless communication systems and radar systems to concentrate their energy toward a specific receiver or target. The electronic beam steering functionality in the transmitters are mainly based on analog beamforming techniques. Adequate phase control of each antenna element is the key technology to implement the beam steering transmitters. The simplest way to feed the optimum phase to the antenna is to use the beamforming network and switches like Buttler matrix [1] or Rotman lens [2]. However, they have demerits of huge size and losses. Instead of the beamforming networks, phase control using the delay controllable material like liquid crystal [3] or BST [4] have been researched, which shows wide angle continuous scanning capability without switches and DC power consumption. However, those approaches are annoyed by the loss especially in mm-wave range and relatively poor mass production capability.

To individually control the phase of each antenna, active phase shifters using PiN diodes have been widely used in transmitting antenna array [5] or transmittance array

The associate editor coordinating the review of this manuscript and approving it for publication was Dušan Grujić.

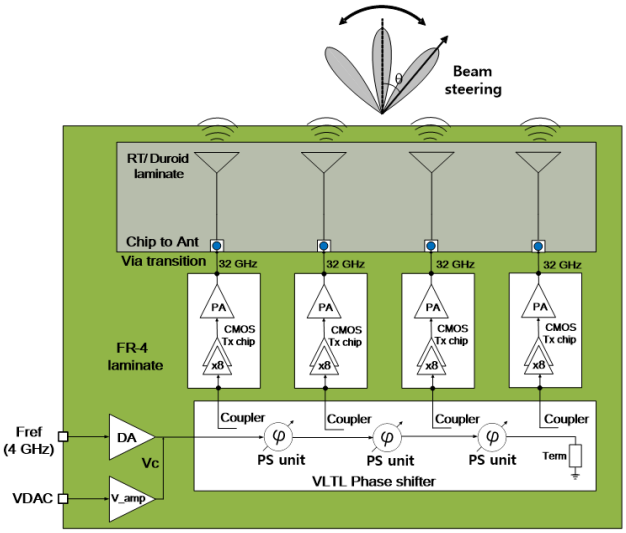

FIGURE 1. Block diagram of the Ka-band 1 × 4 phased array transmitter.

antennas [5], which can achieve a good scanning performance with more manufacturability at more affordable costs, but its application is limited as the operating frequency enters the deep mm-wave range due to packaging with the bias and control networks for PiN diodes.

Nowadays, development of semiconductor technology enables the design of active phased arrays which utilize the integrated on-chip phase shifters [6], [7], [8], [9], [10], [11]. While the active phased array provides multi-functionality such as beam steering, multi-beam radiation and polarization diversity, individual phase control for each channel requires the wide phase control range, the burden of implementation area and the control complexity of the on-chip phase shifters grow especially for massive array application.

One method to reduce the required phase control range for the phase shifter is using a frequency multiplier with a phase shifter that operates at a much lower reference frequency equal to the antenna operating frequency divided by the multiplication ratio [12]. However, it also requires the individual phase shifter and an N-way power distribution network, which might complicate the integration of the massive phase array and limit the channel scalability.

Before the advent of the integrated active phase shifters, the varactor loaded transmission line (VLTL) was developed as a variable delay line [13], [14] and a monolithic distributed analog phase shifter was also reported [15], [16], [17], [18]. The delay or phase of the VLTL is controlled by varying the control voltage of periodically shunt-loaded varactors in the transmission line. The VLTL has several merits such as the broadband characteristic due to true time delay nature, no DC power consumption, and the scalable phase control range by cascading the unit VLTL network [19], [20]. Though the VLTL shows the progressive phase accumulation along the line, which is beneficial to configure the phased array system, implementing multi-phase outputs from a single VLTL for beam steering has not been reported because the periodic loading of the antennas along the VLTL hinders the input matching and equal power distribution to all antenna channels. Besides the difficulty of multi-phase output from a single VLTL, a change of varactor capacitance causes a change of line characteristic impedance and therefore input and output impedance mismatching. Additionally, the insertion loss of the VLTL also increases as the maximum capacitance of the varactor increases. Therefore, VLTLs are merely used to design wideband phase shifters with a single input and single output to configure the phased array antenna system. However, this configuration has no noticeable benefits compared to active phase shifters. Therefore, nowadays, use of VLTLs as phase shifters is not readily considered.

This work presents a compact phased array with a single VLTL phase shifter and a single voltage control while providing multi-phase outputs. At first, adopting the short-coupled line coupler is introduced to extract the multi-phase outputs from a single VLTL to minimize the periodic loading effect and ensure the uniform power distribution. Additionally, using the frequency multiplier minimize the required phase shift, i.e., the amount of varactor capacitance variation at the reference frequency, which mitigates the discontinuity of the periodic loading of varactors along the transmission line. In debt to the new architecture, this work presents an electrically steerable compact Ka-band phased array transmitter using a single VLTL phase shifter. In Section II, detailed configuration of the proposed system is explained with an analysis of the required amount of the phase change of the VLTL. Section III shows the measurement results and conclusions is given in Section IV.

II. ELECTRICALLY STEERABLE KA-BAND PHASED ARRAY TRANSMITTER

Fig. 1 shows a block diagram of the proposed beam steering Ka-band phased array transmitter. The 4 GHz reference input is applied to a single VLTL phase shifter via a driver amplifier and the coupled four phase-accumulated outputs drive CMOS transmitter chips configured with an ×8 frequency multiplier and a Ka-band power amplifier.

A VLTL phase shifter consists of three cascaded unit sections. The external bias voltage through a voltage digital analog converter (VDAC) is boosted 5.7 times by a voltage amplifier mounted on the FR-4 laminate and this amplified voltage is applied as the control voltage V_c of the shunt-loaded varactors.

The radiation beam is electrically steered depending on the phase difference φ_{ant} between adjacent antenna elements. The required phase difference φ_{ant} for the beam steering angle θ is determined by (1).

$$\Delta\varphi_{ant} = 2n\pi + \left(\frac{2\pi}{\lambda}\right) d \sin\theta, \tag{1}$$

where d is the distance between antenna elements, and λ is the wavelength of radiated signal. The required phase shift φ_{ps}

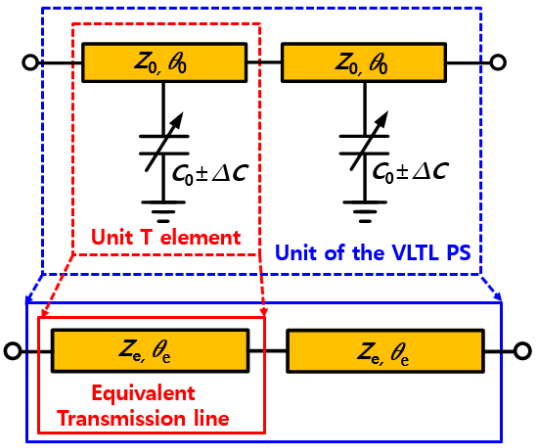

FIGURE 2. Unit element of the coupled varactor loaded transmission line phase shifter.

along the VLTL phase shifter at the reference frequency is reduced by the frequency multiplication ratio m as in (2).

$$\Delta\varphi_{ps} = \frac{1}{m}\left[2n\pi + \left(\frac{2\pi}{\lambda}\right) d\sin\theta\right] \tag{2}$$

A. ANALYSIS OF COUPLED VARACTOR LOADED LINE PHASE SHIFTER

For $m = 8$ in (2), the required phase difference at the reference frequency between adjacent outputs of the VLTL, to realize a maximum beam steering angle of $\pm\theta_{\rm m}$ is

$$\frac{n\pi}{4} \pm \left(\frac{\pi}{4\lambda}\right) d\sin(\theta_m), \tag{3}$$

where the first term determines the electrical length of the unit section between adjacent outputs of the VLTL for the beam looking at the boresight, and the second term is the required phase shift for the maximum beam steering at the reference frequency. Though the weak coupling technique diminishes the periodic loading effects of the transmitters, the loading with the nominal period of 180° at the reference frequency systematically ensures equal power distribution. Therefore, the nominal length of the unit section of the VLTL is selected as the half wavelength at the reference frequency. The unit section of the VLTL is composed of two cascaded T sections, of which the equivalent electrical length is 90°. Since the varactor capacitance changes its value around some offset capacitance C_0, the physical length of the transmission line in the T section should be reduced to $\lambda/4 - \Delta\ell$ due to the loading of C_0 for boresight targeting. The varactor changes its capacitance to $C_0 \pm \Delta C$ according to control voltage for beam steering and the corresponding shunt susceptance B is $B_0 \pm \Delta B$.

Since the coupling between transmitter chip and the VLTL is so weak, the amount of phase change of the VLTL according to the change of the varactor capacitance can be analyzed, ignoring the loading effect of the transmitter chips.

In Fig. 2, the θ_0 and Z_0 are the electrical length and the characteristic impedance of the transmission line in the T section. The electrical length θ_0 is given by

$$\theta_0 = \beta_0(\lambda/4 - \Delta\ell) = \pi/2 - \Delta\theta, \tag{4}$$

where β_0 is the phase constant of the transmission line of the T section and $\Delta\theta = \beta_0\Delta\ell$. Then the ABCD matrix for the unit T delay element can be expressed as (5), as shown at the bottom of the page.

Then the ABCD matrix (5) of the T section is compared to that of the equivalent transmission line (6) to determine the equivalent electrical length $\theta_{\rm e}$ and the line impedance $Z_{\rm e}$.

$$\begin{bmatrix} A & B \\ C & D \end{bmatrix}_e = \begin{bmatrix} \cos\theta_e & jZ_e\sin\theta_e \\ j\frac{\sin\theta_e}{Z_e} & \cos\theta_e \end{bmatrix} \tag{6}$$

By comparing (5) and (6), the reduction length $\Delta\ell$ can be determined for a given offset capacitance C_0. For boresight steering, the equivalent electrical length $\theta_{\rm e}$ of the unit T section should be 90° for $B_0(= \omega_{ref} C_0)$. Therefore, the A parameter of the T element should be zero, and the reduction length $\Delta\ell$ is calculated as

$$\Delta\theta = \beta_0\Delta\ell = \tan^{-1}\left(\frac{B_0 Z_0}{2}\right) \tag{7}$$

Once the length of the transmission line is determined, the line impedance $Z_{\rm e}$ can be determined by comparing two ABCD parameters in terms of the varactor susceptance B.

$$Z_e = \frac{B_T}{\sqrt{A_T^2 - 1}} = \frac{Z_0\left(\cos\Delta\theta + \frac{BZ_0}{2}(\sin\Delta\theta - 1)\right)}{\sqrt{1 - \left(\frac{\Delta BZ_0}{2}\cos\Delta\theta\right)^2}}, \tag{8}$$

where A_T, B_T are the ABCD parameters of the T element and B is the susceptance of the varactor. Finally, the amount of effective phase change $\Delta\theta_{\rm e}$ due to the ΔB is determined by the following condition (9).

$$\begin{aligned}\cos\theta_e &= \cos\left(\frac{\pi}{2} + \Delta\theta_e\right) = -\sin\Delta\theta_e \\ &= \sin\Delta\theta - \frac{(B_0 + \Delta B)Z_0}{2}\cos\Delta\theta = -\frac{\Delta BZ_0}{2}\cos\Delta\theta,\end{aligned} \tag{9}$$

which gives the closed-form result

$$\Delta\theta_e = \sin^{-1}\left(\frac{\Delta BZ_0}{2}\cos\Delta\theta\right) \tag{10}$$

$$\begin{bmatrix} A & B \\ C & D \end{bmatrix}_T = \begin{bmatrix} \left(\sin\Delta\theta - \frac{BZ_0}{2}\cos\Delta\theta\right) & jZ_0\left(\cos\Delta\theta + \frac{BZ_0}{2}(\sin\Delta\theta - 1)\right) \\ jY_0\left(\cos\Delta\theta + \frac{BZ_0}{2}(\sin\Delta\theta + 1)\right) & \left(\sin\Delta\theta - \frac{BZ_0}{2}\cos\Delta\theta\right) \end{bmatrix} \tag{5}$$

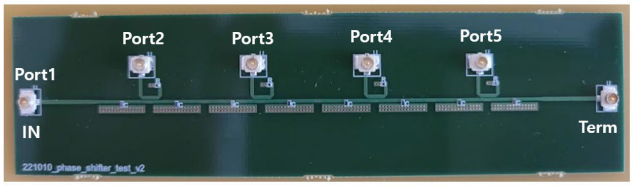

FIGURE 3. Prototype of the coupled varactor loaded transmission line phase shifter.

To evaluate the design equations from (7) to (10), the commercially available varactor MACOM MAVR-000120 is used, which has the capacitance variation about from 140 to 920 fF. At first, it is necessary to determine the offset capacitance C_0. Considering the return loss of the unit T section, the value of C_0 should be as low as possible. However, the value of C_0 should afford the maximum decrement of ΔC to support the required phase change. With few iterations, the offset capacitance C_0 is chosen as 280 fF. Then, using (7), the reduction angle $\Delta\theta$ of a unit T section is determined to be 9.98° to achieve the equivalent electrical length θ_e for 90° phase shift.

To achieve a maximum beam steering angle of ±20° for the antenna element spacing d of 0.7λ, the total phase shift of the unit section of the VLTL should change from 169° and 191° at the reference frequency. Then, the corresponding effective phase change $\Delta\theta_e$ of the unit T section is 5.5° which is accomplished by the varactor capacitance change ΔC of 141.3 fF using (10) at the reference frequency of 4 GHz. For the varactor capacitance variation from 138.7 to 421.3 fF, the calculated Z_e is 45.8 and 38.5 Ω respectively by (8), which ensures the return loss more than 17 dB.

These analysis results in good agreement with the S-parameter simulation results under 50 Ω termination based on the VLTL phase shifter unit model shown in Fig. 2, which showed the results of the 169° phase shift under 138 fF varactor capacitance and the 191° phase shift under 430 fF varactor capacitance.

B. VLTL PHASE SHIFTER PROTOTYPE

Fig. 3 is a fabricated VLTL phase shifter prototype to verify the operation and performance. Anritsu MS 4647A network analyzer is used to measure the phase change, return, and insertion losses as a function of the varactor control voltage V_c, which is applied to the VLTL using the bias-tee.

Fig. 4(a) shows the phase difference between adjacent two outputs as a function of V_c at 4 GHz reference frequency. When V_c varies from 2 to 12 V, the average amount of phase change of unit phase shifter sections is 37.7°. The required phase difference ranges from 169° to 191° for θ_m of ±20° is achieved for a control voltage V_c between 3.4 and 12 V, which gives the varactor capacitance approximately 430 and 175 fF respectively according to MACOM's document. The experimentally estimated varactor capacitance for beam steering is close to the theoretical calculation based on the analysis model in Fig. 2. This result implies that the phase control

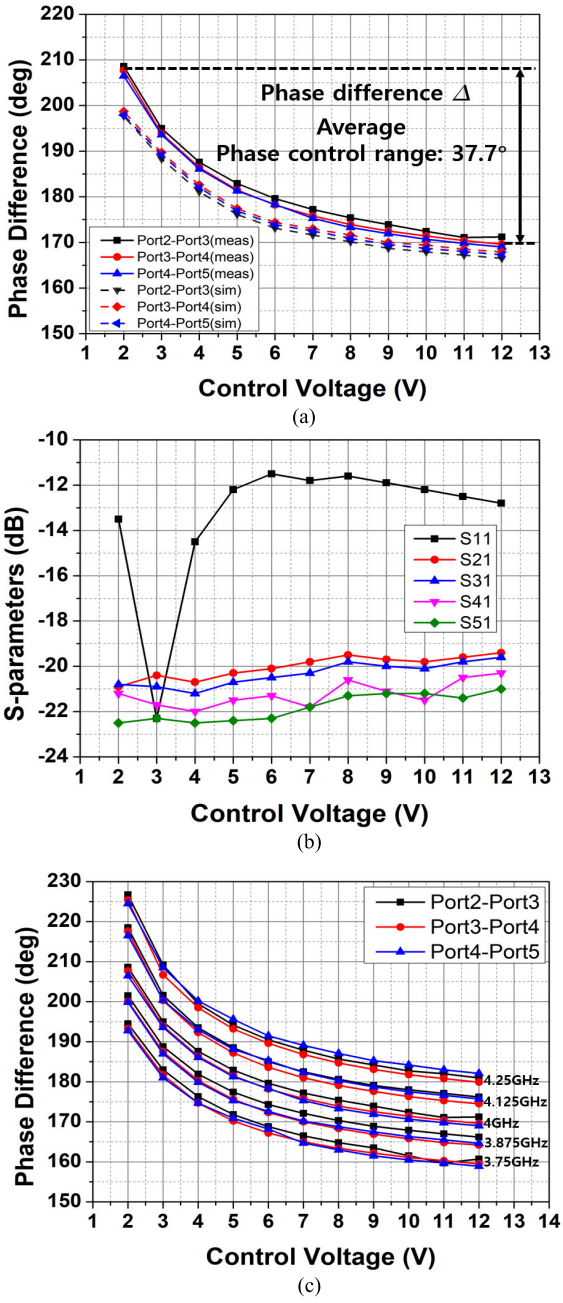

FIGURE 4. Measurement results of the VLTL phase shifter prototype. (a) Phase difference versus control voltage at 4 GHz, (b) S-parameters versus control voltage at 4 GHz, (c) Phase difference versus control voltage and versus frequency.

characteristics of the proposed coupled VLTL phase shifter can be used ignoring the loading effect of the transmitter chips.

The network parameters from the input to the four outputs are measured under the range of V_c from 2 to 12 V. The measured return loss at the input port is between 11.5 and 22.3 dB, and an insertion loss is between 19.4 and 22.5 dB, as shown in Fig. 4(b). The mismatch of insertion loss among four channels is caused by the finite return loss of the unit phase shifting section and attenuation along the

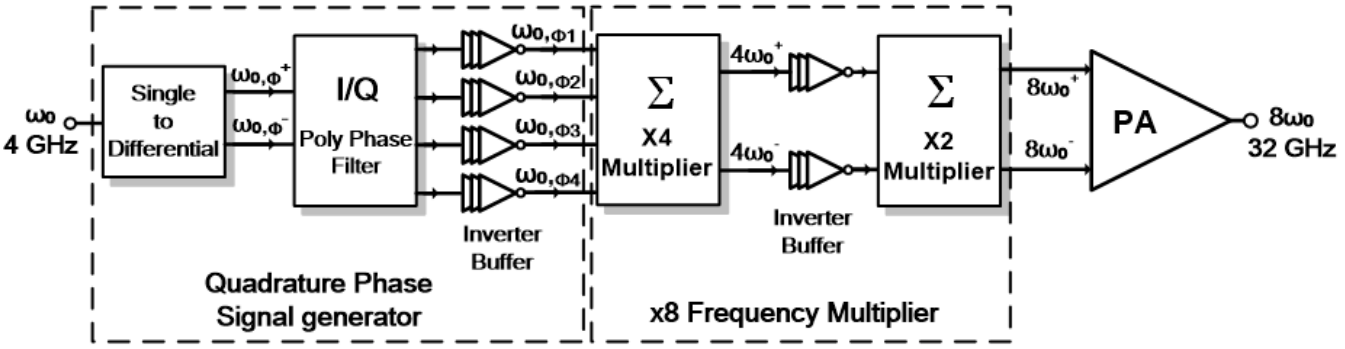

FIGURE 5. Block diagram of the CMOS transmitter chip.

transmission line. The systematic mismatch of the insertion loss can be improved by optimizing the coupling ratio of each coupler. In this work, the sufficient gain of the inverter buffer in the transmitter chip ensures rail-to-rail swing at the input of the ×8 frequency multiplier, which partially compensates for mismatches of the input driving power strength among transmitter chips. Fig. 4(c) is the measurement results of the phase difference between adjacent outputs according to the input frequency variation of ±0.125 GHz steps around 4 GHz. It shows that the phase difference increases as the frequency increases. The phase control range is proportional to the input frequency, with an average value of 33.8° at 3.75 GHz and 44.5° at 4.25 GHz.

C. CMOS TRANSMITTER CHIP DESIGN

Fig. 5 shows the block diagram of the CMOS transmitter chip for the Ka-band beam steering transmitter module. The chip is fabricated using a 28-nm CMOS SOI technology and consists of a quadrature phase signal generator, ×8 frequency multiplier, and a Ka-band power amplifier. By the frequency multiplication ratio of 8, an external single-ended input signal for the final output frequency of 32 GHz is about 4 GHz. The single-ended input signal is converted to the four- phase signals through the transformer balun and the RC poly-phase filter as shown in Fig. 6(a). A compact-sized inverter buffer chain is inserted between the four-phase signal generator and the ×8 frequency multiplier without a separate impedance matching network that demands a large implementation area at the reference input frequency around 4 GHz. The inverter buffer compensates for the loss of the RC poly-phase filter and enhance the signal up to a rail-to-rail output voltage swing. The quadrupler, the first stage of the ×8 frequency multiplier, combines the four-phase signals in the current domain and converts the fourth harmonic current to the voltage signal using a single transformer load connected to common drain nodes of four complementary push-push cells [21]. The quadrupler consumes the much smaller area compared to the cascading of two frequency doublers. The final frequency doubler stage also adopts the complementary push-push doubler structure [21] and its differential output is

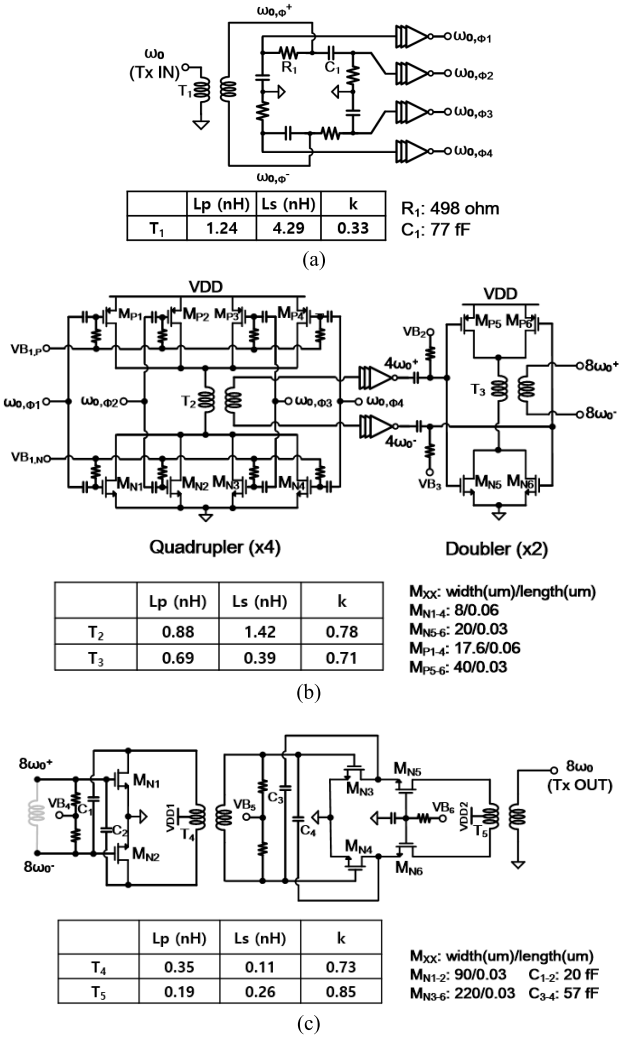

	Lp (nH)	Ls (nH)	k
T_1	1.24	4.29	0.33

R_1: 498 ohm
C_1: 77 fF

	Lp (nH)	Ls (nH)	k
T_2	0.88	1.42	0.78
T_3	0.69	0.39	0.71

M_{XX}: width(um)/length(um)
M_{N1-4}: 8/0.06
M_{N5-6}: 20/0.03
M_{P1-4}: 17.6/0.06
M_{P5-6}: 40/0.03

	Lp (nH)	Ls (nH)	k
T_4	0.35	0.11	0.73
T_5	0.19	0.26	0.85

M_{XX}: width(um)/length(um)
M_{N1-2}: 90/0.03 C_{1-2}: 20 fF
M_{N3-6}: 220/0.03 C_{3-4}: 57 fF

FIGURE 6. Schematic of the transmitter chip configuration blocks. (a) Quadrature phase signal generator, (b) x8 frequency multiplier, (c) Ka-band power amplifier.

transmitted to the Ka-band power amplifier. The quadrupler output is coupled to the inverter buffer chain through the transformer, which is designed to have resonance at the fourth

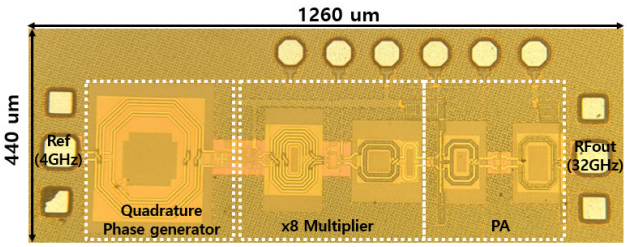

FIGURE 7. Microphotograph of the fabricated transmitter chip.

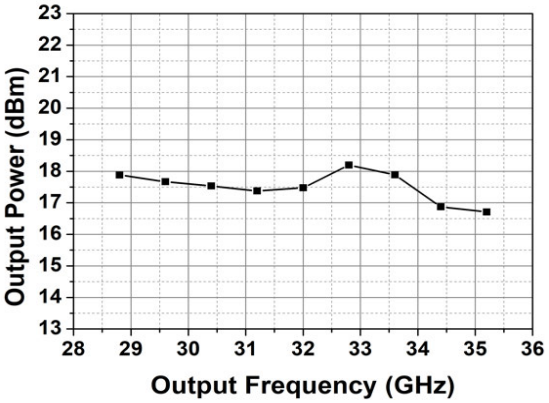

FIGURE 8. Output power measurement results of the fabricated transmitter chip.

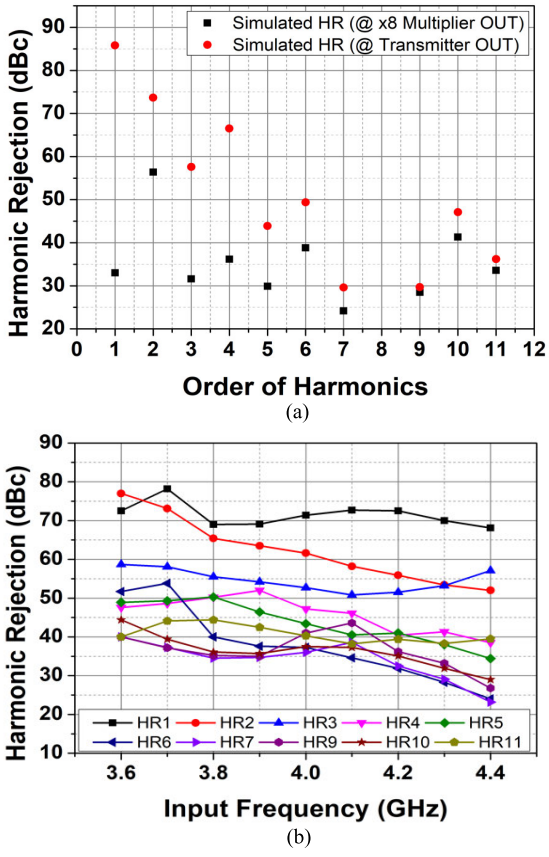

FIGURE 9. (a) Simulated harmonic rejection at the outputs of the x8 frequency multiplier and transmitter with the input frequency of 4 GHz, (b) Measured harmonic rejection versus input frequency at the transmitter output.

harmonic frequency at the primary input of the transformer reflecting the input capacitance of the inverter chain. The inverter output directly drives the succeeding complementary push-push doublers [21] without a matching network because the inverter chain enables the rail-to-rail swing at the input of the following doubler, and the higher order harmonics are sufficiently suppressed due to the limited bandwidth. Fig. 6(c) shows the schematic of the Ka-band power amplifier to amplify the $\times 8$ frequency multiplier output signal power. The two-stage PA consists of a driver stage with a differential CS structure and a power stage with a differential cascode structure for high gain and output power performance. All impedance matching networks are designed with a transformer coupling structure and all stages employ cross-coupled neutralization capacitance to improve stability and gain [22].

The die micrograph of the fabricated transmitter chip is shown in Fig. 7. The chip size is 1.26 mm $\times$ 0.44 mm including all pads. Fig. 8 shows the on-wafer probing measurement result of the transmitter output power according to the reference input frequency variation. A reference input signal of 3 dBm is applied to the transmitter chip input port at 0.1 GHz step from 3.6 to 4.4 GHz. The measured maximum output power is 18.2 dBm at 32.8 GHz and 17.5 dBm at 32 GHz. The deviation of measured output power from 28.8 to 35.2 GHz is only 1.5 dB, achieving broadband output power performance. Fig. 9 shows the simulation and measurement results for the harmonic rejection performance of a transmitter at input power of 3 dBm. In Fig. 9(a), the simulated minimum harmonic rejection at the outputs of the $\times 8$ frequency multiplier and transmitter, for a reference input frequency of 4 GHz, is 24.2 dBc and 29.6 dBc, respectively. The measured minimum harmonic rejection at the transmitter output is 23.2 dBc within the measured input frequency range and 36 dBc at the reference input frequency of 4 GHz, as shown in Fig. 9(b).

D. ARRAY ANTENNAS DESIGN AND INTEGRATION OF PHASED ARRAY TRANSMITTER

This section describes the 1×4 array antenna design and the build of the phase shifter, transmitter chips, and array antennas into a phased array transmitter module. By using a conductive epoxy, the ground plane of RT/Duroid laminate with patch array antennas on top is attached to the ground plane of the 4-layer FR-4 laminate in which a phase shifter, driver amplifier, voltage amplifier, and DC bias electrode are implemented. As shown in Fig. 10, an air cavity is formed on FR-4 laminate to mount a transmitter chip on the exposed ground plane of the RT/Duroid laminate. To connect each output of the phase shifter to each transmitter chip, which is spaced equal to the distance between adjacent antenna elements ($d = 0.7\lambda$), four identical 50 Ω Grounded Coplanar

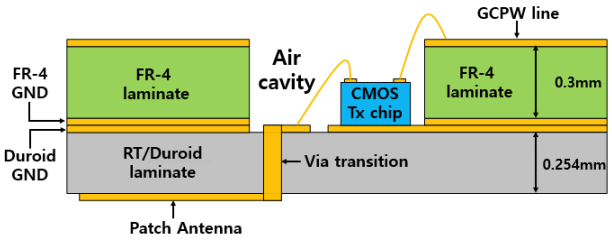

FIGURE 10. Cross section of the stacked FR-4 and RT/Duroid laminate.

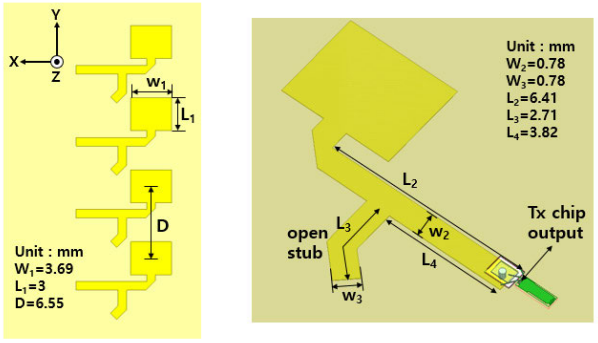

FIGURE 11. (a) Top view of the 1 × 4 patch array antennas, (b) Transition network between transmitter chip and patch antenna.

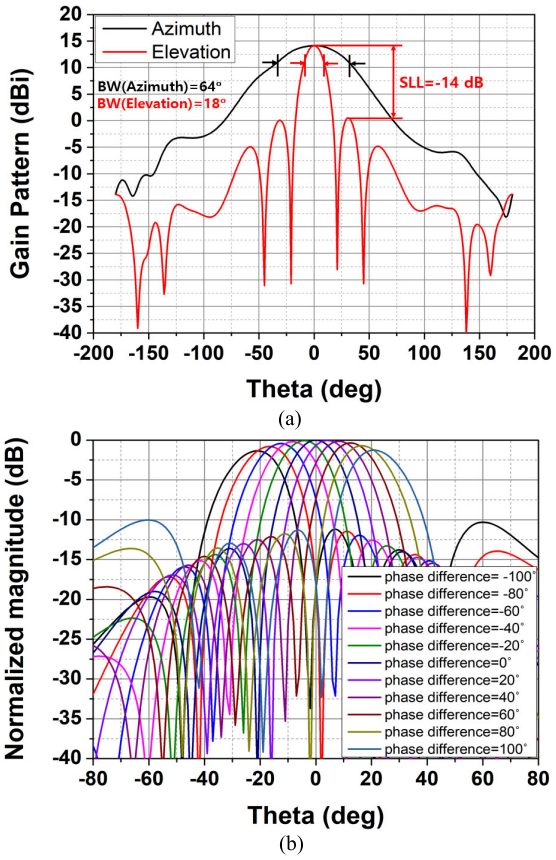

FIGURE 12. Simulation results of the 1 × 4 array antennas at 32 GHz. (a) E- and H-plane patterns, (b) Beam steering pattern in E-plane.

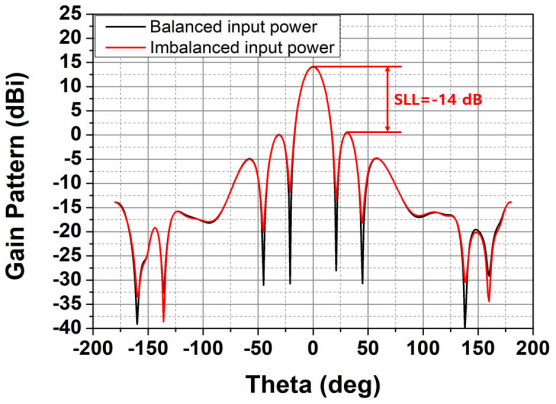

FIGURE 13. Simulation results of elevation radiation pattern for 1 × 4 array antennas with and without input power imbalance (maximum 2.1 dB among four antennas) at 32 GHz.

Waveguide (GCPW) lines are implemented on FR-4 laminate. The end of the line is connected to the transmitter chip input by wire bonding in the air cavity.

Fig. 11(a) shows the patch array antennas designed on RT/Duroid laminates. For the 1 × 4 vertical array, each antenna element has a patch antenna fed by the microstrip line bent by 90°. The open stub for impedance matching is bent by 45° to minimize the mutual influence on the radiation characteristics between adjacent antenna elements. Each antenna element is designed the same and placed at 0.7λ from center to center. Fig. 11(b) shows the Ka-band signal transition network between the transmitter chip output and the patch antenna. The output signal of the chip is transmitted to the patch antenna through wire bonding, through-hole via penetrating RT/Duroid laminate, and microstrip feeding line.

Fig. 12 shows the simulation results of E- and H-plane radiation patterns and E-plane beam steering characteristics of the designed 1 × 4 array antennas. To verify the antenna radiation patterns with full 3D-EM simulations, the input signal is set to be fed from the chip output as in Fig. 11(b). As shown in Fig. 12(a), the designed array antennas achieved a 14.1 dBi gain at a 0° scan angle, and a 3-dB beam width of 64° (azimuth) × 18° (elevation). The sidelobe levels are -14 dB or less. Based on (1), the demanded phase difference of input signals between adjacent antenna elements is $2\pi n \pm 0.48\pi$ ($=360°n \pm 86.4°$) to realize the target maximum beam steering angle (θ_m) of ±20°.

The simulation results of the beam steering in the E-plane are shown in Fig. 12(b) with the phase difference between array antenna inputs increased from −100° to +100° by 20°.

When signals with a phase difference of -100° are fed to each element sequentially from the topmost antenna in Fig. 11(a), a beam steering angle of -22° in the E-plane is obtained.

TABLE 1. Performance comparison with previous phased array transmitter for beam steering.

Parameter	[12]	[23]	[24]	[25]	[26]	[27]	This work
Tx array	2×2	4×8	8×1	8×4	8×1	8×8	1×4
Technology	65-nm CMOS	0.18-um SiGe BiCMOS	65-nm CMOS	65-nm CMOS + 0.15-um E-mode GaAs pHEMT	0.18-um SiGe BiCMOS	0.18-um SiGe BiCMOS	28-nm CMOS
Antenna integration	In Package	In Package	On separate PCB	In Package	In Package	In Package	In Package
Phase shifter configuration	Multi	Multi	Multi	Multi	Multi	Multi	Single
Phase control/ Resolution	Analog/ Continuos	Digital/ 6 bit	Digital/ 2+3+10 bit	Digital/ 4 bit	Digital/ 5 bit	Digital/ 6 bit	Analog/ Continuos
Required phase shifter control range (°)	200°*	360°	360°	360°	360°	360°	21.5°****
Psat/ch (dBm)	-	13	18	23.8	14.4-15.3	12	17.5
Peak EIRP (dBm)	29.4	41**	39.8	47.5** (include GaAs PA)	34.5	51	38.1
DC Power (W)	1.2	6.4**	2.4#	34.1**	2**	18	5.7†
Beam steering (°)	±9° -H ±7° -E	±50° -H ±20° -E	±50° -H(only)	±60° -H ±30° -E	±60° -H(only)	±60° -H ±50° -E	±20° -E(only)
Frequency (GHz)	88.5-98.5	27.8-31.2	28	37-38.8***	19.5-51	36-41.5	30-32.4
Fractional BW (%)	10.8	11.5	-	4.7	78.8	13.8	7.6

* Commercial phase shifter die(Hittite HMC247), typical phase shift range. ** At OP1dB. *** Graphically estimated from the reported figures. **** Single phase shifter unit, at the reference frequency. # At 7 dB back-off from Psat. † Include all peripheral circuits(LDOs and DA on FR-4).

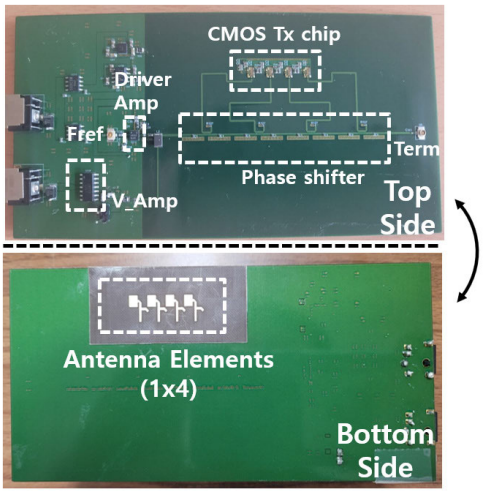

FIGURE 14. Top and bottom views of the fabricated 1 × 4 phased array transmitter module.

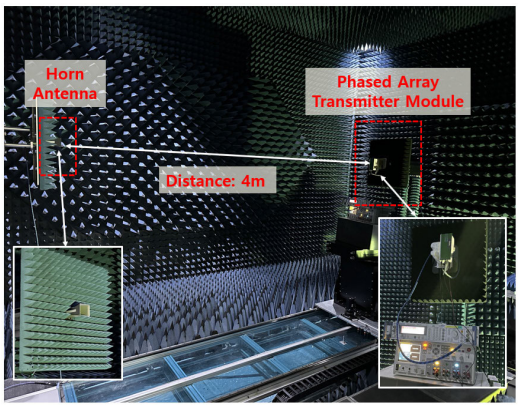

FIGURE 15. Beam pattern measurement setup.

On the other hand, when signals with +100° phase difference are sequentially applied, a beam steering angle of +22° is obtained. The 3-dB beam width of 18° is achieved consistently across the steering angles. To examine the effects of input power imbalance of the four array antennas due to the mismatch of the insertion loss shown in Fig. 4(b), the elevation radiation pattern is simulated using the measured mismatch. As shown in Fig. 13, noticeable difference in the

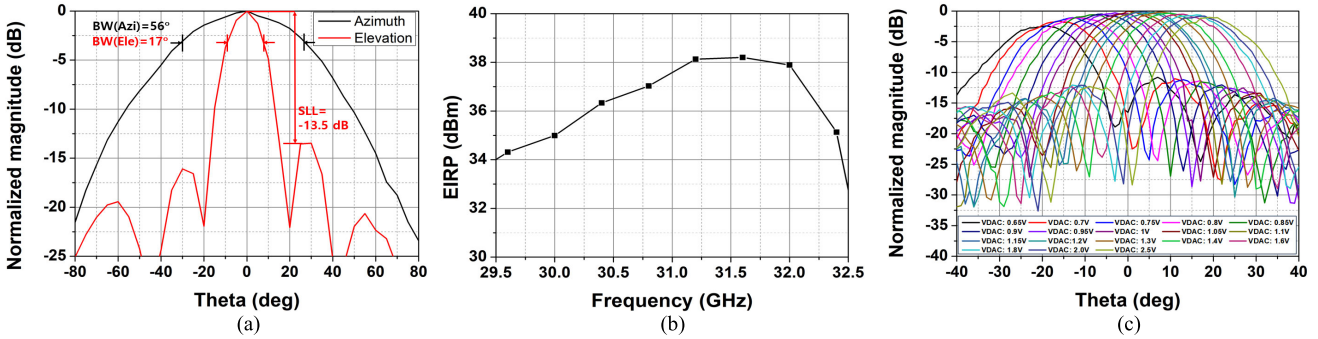

FIGURE 16. Measurement results of the fabricated 1 × 4 phased array transmitter. (a) E- and H-plane beam patterns at 32 GHz, (b) EIRP versus frequency, (c) Beam steering pattern in E-plane at 32 GHz.

side lobe level is not observed for the maximum mismatch of 2.1 dB.

III. PHASED ARRAY TRANSMITTER MODULE MEASUREMENT RESULTS

Fig. 14 shows a Ka-band 1 × 4 phased array transmitter module manufactured by attaching FR-4 and RT/Duroid laminate. Fig. 15 shows a setup for beam pattern measurement. The beam pattern of the proposed phased array transmitter is evaluated with a 23 dBi horn antenna at a 4 m distance. The measurement results of the normalized beam patterns of the E- and H-planes as a function of beam scan angle at 32 GHz are shown in Fig. 16(a). A 3-dB beam width of 17° in the E-plane and 56° in the H-plane is achieved, and the measured sidelobe levels are below −13.5 dB at all scan angles. In addition, the peak-to-null ratios in the E-plane are at least 22 dB at 0° scan angle. Fig. 16(b) shows measurement results of the effective isotropic radiated power (EIRP) according to frequency variation at the saturated transmitter chip output power. A peak EIRP of 38.1 dBm is achieved at 31.6 GHz, and the measured 3-dB bandwidth is 2.4 GHz between 30 and 32.4 GHz. The measured normalized beam pattern for E-plane beam steering at 32 GHz is shown in Fig. 16(c). By achieving a beam steering angle of -20° at a VDAC bias voltage of 0.65 V (V_c: 3.71 V) and beam steering angle of 20° at a VDAC bias voltage of 2.5 V (V_c: 14.3 V), the proposed phased array transmitter shows ± 20° maximum beam steering capability in the E-plane.

Performance comparison with a recent state-of-art phased array transmitter for beam steering is shown in Table 1. Although wider beam steering angles have been reported in other studies, the phase shifter control complexity are high due to the configuration of individual phase shifters for each channel [12], [23], [24], [25], [26], [27]. Also, a phase shifter with a 360° complete control range is used [23], [24], [25], [26], [27]. The proposed phased array structure enables inherent phase-accumulating operation between multiple outputs of the phase shifter and has a built-in frequency multiplier. The required phase control range of the phase shifter unit to realize a beam steering angle of ±20° with the proposed phased array structure is approximately only 21.5° at the reference frequency. According to (3), it can be possible to achieve a ±60° beam steering angle with a small phase control range of 54.5° for VLTL phase shifter unit.

IV. CONCLUSION

This work presents a Ka-band 1 × 4 beamforming transmitter using a coupled varactor loaded line phase shifter. Through the integration with a frequency multiplier and a coupler, the varactor loaded transmission line can be effectively used as a phase shifter, providing multi-phase outputs. Additionally, the accurate design equation is derived and experimentally confirmed. Since the proposed phased array structure utilizes inherent phase accumulation along the single transmission line, there is no difficulty of a complicated phase calibration procedure as the number of the array elements increases. Therefore, infinite scalability and continuous beamforming capability are ensured.

ACKNOWLEDGMENT

The chip fabrication and EDA tools were supported by the Integrated circuit Design Education Center (IDEC), South Korea.

REFERENCES

[1] A. Tajik, A. S. Alavijeh, and M. Fakharzadeh, "Asymmetrical 4 × 4 Butler matrix and its application for single layer 8 × 8 Butler matrix," *IEEE Trans. Antennas Propag.*, vol. 67, no. 8, pp. 5372–5379, Aug. 2019.

[2] W. Lee, J. Kim, and Y. J. Yoon, "Compact two-layer Rotman lens-fed microstrip antenna array at 24 GHz," *IEEE Trans. Antennas Propag.*, vol. 59, no. 2, pp. 460–466, Feb. 2011.

[3] H. Kim and S. Nam, "Performance improvement of LC-based beam-steering leaky-wave holographic antenna using decoupling structure," *IEEE Trans. Antennas Propag.*, vol. 70, no. 4, pp. 2431–2438, Apr. 2022.

[4] M. Nikfalazar, M. Sazegar, A. Mehmood, A. Wiens, A. Friederich, H. Maune, J. R. Binder, and R. Jakoby, "Two-dimensional beam-steering phased-array antenna with compact tunable phase shifter based on BST thick films," *IEEE Antennas Wireless Propag. Lett.*, vol. 16, pp. 585–588, 2017.

[5] F. F. Manzillo, M. Smierzchalski, J. Reverdy, and A. Clemente, "A Ka-band beam-steering transmitarray achieving dual-circular polarization," in *Proc. 15th Eur. Conf. Antennas Propag. (EuCAP)*, Dusseldorf, Germany, Mar. 2021, pp. 1–4.

[6] X. Luo, J. Ouyang, Z.-H. Chen, Y. Yan, L. Han, Z. Wu, T. Yu, and K. Zheng, "A scalable Ka-band 1024-element transmit dual-circularly-polarized planar phased array for SATCOM application," *IEEE Access*, vol. 8, pp. 156084–156095, 2020.

[7] K. Kibaroglu, M. Sayginer, T. Phelps, and G. M. Rebeiz, "A 64-element 28-GHz phased-array transceiver with 52-dBm EIRP and 8–12-Gb/s 5G link at 300 meters without any calibration," *IEEE Trans. Microw. Theory Techn.*, vol. 66, no. 12, pp. 5796–5811, Dec. 2018.

[8] Y. Wang et al., "A 39-GHz 64-element phased-array transceiver with built-in phase and amplitude calibrations for large-array 5G NR in 65-nm CMOS," *IEEE J. Solid-State Circuits*, vol. 55, no. 5, pp. 1249–1269, May 2020.

[9] W. Zhu, J. Wang, X. Zhang, W. Lv, B. Liao, Y. Zhu, and Y. Wang, "A 24–28-GHz four-element phased-array transceiver front end with 21.1%/16.6% transmitter peak/OP1dB PAE and subdegree phase resolution supporting 2.4 Gb/s in 256-QAM for 5-G communications," *IEEE Trans. Microw. Theory Techn.*, vol. 69, no. 6, pp. 2854–2869, Jun. 2021.

[10] B. Sadhu, A. Paidimarri, W. Lee, M. Yeck, C. Ozdag, Y. Tojo, J.-O. Plouchart, X. Gu, Y. Uemichi, S. Chakraborty, Y. Yamaguchi, N. Guan, and A. Valdes-Garcia, "A 24-to-30 GHz 256-element dual-polarized 5G phased array with fast beam-switching support for >30,000 beams," in *IEEE Int. Solid-State Circuits Conf. (ISSCC) Dig. Tech. Papers*, vol. 65, Feb. 2022, pp. 436–438.

[11] S. Shakib, M. Elkholy, J. Dunworth, V. Aparin, and K. Entesari, "A wideband 28-GHz transmit–receive front-end for 5G handset phased arrays in 40-nm CMOS," *IEEE Trans. Microw. Theory Techn.*, vol. 67, no. 7, pp. 2946–2963, Jul. 2019.

[12] R. Klimovich, S. Jameson, and E. Socher, "W-band endfire 2-D phased-array transmitter based on ×9 CMOS active multiplier chips," *IEEE Trans. Antennas Propag.*, vol. 68, no. 12, pp. 7893–7904, Dec. 2020.

[13] E. K. Kirchner, "Microwave variable delay devices," *IEEE Trans. Microw. Theory Techn.*, vol. MTT-17, no. 11, pp. 986–997, Nov. 1969.

[14] H. Weinstein, "Linear signal stretching in a time-variant system," *IEEE Trans. Circuit Theory*, vol. CT-12, no. 2, pp. 157–164, Jun. 1965.

[15] W. A. Davis, "Design equations and bandwidth of loaded-line phase shifters (short papers)," *IEEE Trans. Microw. Theory Techn.*, vol. MTT-22, no. 5, pp. 561–563, May 1974.

[16] J. F. White, "High power, p-i-n diode controlled, microwave transmission phase shifters," *IEEE Trans. Microw. Theory Techn.*, vol. MTT-13, no. 2, pp. 233–242, Mar. 1965.

[17] M. E. Davis, "Integrated diode phase-shifter elements for an X-band phased-array antenna (short papers)," *IEEE Trans. Microw. Theory Techn.*, vol. MTT-23, no. 12, pp. 1080–1084, Dec. 1975.

[18] E. C. Niehenke, V. V. DiMarco, and A. Friedberg, "Linear analog hyperabrupt varactor diode phase shifters," in *IEEE MTT-S Int. Microw. Symp. Dig.*, St. Louis, MO, USA, Jun. 1985, pp. 657–660.

[19] F. Ellinger, R. Vogt, and W. Bachtold, "Ultra compact, low loss, varactor tuned phase shifter MMIC at C-band," *IEEE Microw. Wireless Compon. Lett.*, vol. 11, no. 3, pp. 104–105, Mar. 2001.

[20] F. Ellinger, H. Jackel, and W. Bachtold, "Varactor-loaded transmission-line phase shifter at C-band using lumped elements," *IEEE Trans. Microw. Theory Techn.*, vol. 51, no. 4, pp. 1135–1140, Apr. 2003.

[21] J.-H. Park, D.-Y. Yang, K.-J. Choi, and B.-S. Kim, "D-band ×8 frequency multiplier using complementary differential frequency doubler," *IEEE Microw. Wireless Technol. Lett.*, vol. 33, no. 3, pp. 311–314, Mar. 2023.

[22] W. Ye, K. Ma, K. S. Yeo, and Q. Zou, "A 65 nm CMOS power amplifier with peak PAE above 18.9% from 57 to 66 GHz using synthesized transformer-based matching network," *IEEE Trans. Circuits Syst. I, Reg. Papers*, vol. 62, no. 10, pp. 2533–2543, Oct. 2015.

[23] K. Kibaroglu, M. Sayginer, and G. M. Rebeiz, "An ultra low-cost 32-element 28 GHz phased-array transceiver with 41 dBm EIRP and 1.0–1.6 Gbps 16-QAM link at 300 meters," in *Proc. IEEE Radio Freq. Integr. Circuits Symp. (RFIC)*, Honolulu, HI, USA, Jun. 2017, pp. 73–76.

[24] J. Pang et al., "A 28-GHz CMOS phased-array transceiver based on LO phase-shifting architecture with gain invariant phase tuning for 5G new radio," *IEEE J. Solid-State Circuits*, vol. 54, no. 5, pp. 1228–1242, May 2019.

[25] C.-N. Chen, Y.-H. Lin, L.-C. Hung, T.-C. Tang, W.-P. Chao, C.-Y. Chen, P.-H. Chuang, G.-Y. Lin, W.-J. Liao, Y.-H. Nien, W.-C. Huang, T.-Y. Kuo, K.-Y. Lin, T.-W. Huang, Y.-C. Lin, H.-C. Lu, T.-H. Tsai, and H. Wang, "38-GHz phased array transmitter and receiver based on scalable phased array modules with endfire antenna arrays for 5G MMW data links," *IEEE Trans. Microw. Theory Techn.*, vol. 69, no. 1, pp. 980–999, Jan. 2021.

[26] A. Alhamed, G. Gültepe, and G. M. Rebeiz, "A multi-band 16–52-GHz transmit phased array employing 4 × 1 beamforming IC with 14–15.4-dBm P_{sat} for 5G NR FR2 operation," *IEEE J. Solid-State Circuits*, vol. 57, no. 5, pp. 1280–1290, May 2022.

[27] Y. Yin, S. Zihir, T. Kanar, Q. Ma, H. Chung, L. Gao, and G. M. Rebeiz, "A 37–42-GHz 8 × 8 phased-array with 48–51-dBm EIRP, 64-QAM 30-Gb/s data rates, and EVM analysis versus channel RMS errors," *IEEE Trans. Microw. Theory Techn.*, vol. 68, no. 11, pp. 4753–4764, Nov. 2020.

KYU-JIN CHOI (Graduate Student Member, IEEE) received the B.S. and M.S. degrees in electronic, electrical and computer engineering from Sungkyunkwan University, Suwon, South Korea, in 2010 and 2011, respectively, where he is currently pursuing the Ph.D. degree in electronic, electrical and computer engineering. His current research interests include RF and millimeter-wave integrated circuits for wireless communications and radar systems.

REEM SONG (Member, IEEE) received the Ph.D. degree in electrical engineering from the University of Southern California at Los Angeles, Los Angeles, CA, USA, in 2006. From 2007 to 2010, she was a Senior Design Engineer with Skyworks Solutions, Inc., Thousand Oaks, CA, USA. Since 2014, she has been with Sungkyunkwan University, Suwon, South Korea, as a Research Faculty. Her research interests include millimeter-wave circuits, antennas, and systems.

CHAN-JONG LEE received the B.S. degree in electronic engineering from Suwon University, Suwon, South Korea, in 2021, and the M.S. degree in electronic, electrical and computer engineering from Sungkyunkwan University, Suwon, in 2023. He is currently with LG Electronics Inc., Seoul, South Korea. His research interests include millimeter-wave antenna and systems.

JEONG-BAE YOON (Student Member, IEEE) received the B.S. degree in electronic, electrical and computer engineering from Sungkyunkwan University, Suwon, South Korea, in 2021, where he is currently pursuing the Ph.D. degree in electronic, electrical and computer engineering. His current research interests include millimeter-wave circuits, antennas, and systems.

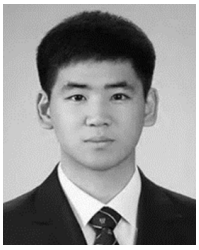

DONG-YEOL YANG (Student Member, IEEE) received the B.S. degree in electrical and electronics engineering from Konkuk University, Seoul, South Korea, in 2020. He is currently pursuing the Ph.D. degree in electronic, electrical and computer engineering with Sungkyunkwan University. His current research interest includes millimeter-wave integrated circuits for radar systems.

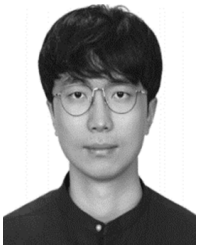

SEUK-WON KANG (Student Member, IEEE) received the B.S. degree in electronics engineering from Kwangwoon University, Seoul, South Korea, in 2021. He is currently pursuing the Ph.D. degree in electronic, electrical and computer engineering with Sungkyunkwan University. His current research interest includes millimeter-wave integrated circuits for radar systems.

SANGWOOK NAM (Senior Member, IEEE) received the B.S. degree in electrical engineering from Seoul National University, Seoul, South Korea, in 1981, the M.S. degree in electrical engineering from Korea Advanced Institute of Science and Technology, Seoul, in 1983, and the Ph.D. degree in electrical engineering from The University of Texas at Austin, Austin, TX, USA, in 1989. From 1983 to 1986, he was a Researcher with the Gold Star Central Research Laboratory, Seoul. Since 1990, he has been a Professor with the School of Electrical Engineering and Computer Science, Seoul National University. His current research interests include analysis/design of electromagnetic structures, antennas, and microwave active/passive circuits.

BYUNG-SUNG KIM (Member, IEEE) received the B.S., M.S., and Ph.D. degrees in electronic engineering from Seoul National University, Seoul, South Korea, in 1989, 1991, and 1997, respectively. In 1997, he joined the College of Information and Communication Engineering, Sungkyunkwan University, Suwon, South Korea, where he is currently a Professor. He was a Visiting Researcher with the University of California at Santa Barbara, Santa Barbara, CA, USA, in 2013. His research interests include high-frequency device modeling and RF/millimeter-wave CMOS integrated circuit design.